RSC Advances

PAPER

Cite this: *RSC Adv.*, 2015, **5**, 88703

# Rational synthesis of zerovalent iron/bamboo charcoal composites with high saturation magnetization†

Mingshan Wu,[ab] Jianfeng Ma,[a] Zhiyong Cai,[c] Genlin Tian,[a] Shumin Yang,[a] Youhong Wang[b] and Xing'e Liu*[a]

The synthesis of magnetic biochar composites is a major new research area in advanced materials sciences. A series of magnetic bamboo charcoal composites (MBC800, MBC1000 and MBC1200) with high saturation magnetization ($M_s$) was fabricated in this work by mixing bamboo charcoal powder with an aqueous ferric chloride solution and subsequently pyrolyzing under different temperatures (800, 1000 and 1200 °C) in a tube furnace. All the products were characterized using X-ray powder diffraction (XRD), X-ray photoelectron spectroscopy (XPS), field emission scanning electron microscopy (FESEM), energy dispersive X-ray spectrometer (EDAX), high-resolution transmission electron microscopy (HRTEM), Raman spectroscopy and a superconducting quantum interference device (SQUID). The results show that the pyrolytic temperature plays a significant role in determining the final structures and magnetic properties of the products. The magnetite ($Fe_3O_4$) and a certain amount of amorphous hematite ($\alpha$-$Fe_2O_3$) coexist in MBC800. However, zerovalent iron (ZVI) is the only detectable magnetic phase in both MBC1000 and MBC1200. The $M_s$ values of MBC1000 and MBC1200 are 118.1 and 122.7 emu $g^{-1}$, respectively. Excellent magnetic properties of the two ZVI/bamboo charcoal composites not only facilitate the separation of solid phase, but also indicate that these materials could have high potential for other applications, such as in the biomedical or ferrofluid fields.

Received 7th July 2015
Accepted 13th October 2015

DOI: 10.1039/c5ra13236c

www.rsc.org/advances

## 1. Introduction

Biochar is increasingly thought of as a multifunctional material and extensively studied for agricultural and environmental applications.[1] Recent reports show that biochar is suitable for contaminant removal because of its surface effective functional groups and high adsorption potential.[2–5] However, it is difficult to separate exhausted biochar from aqueous solutions owing to the small particle size.[1] Hence, separation of these particles typically requires time-consuming processes, such as filtration and centrifugation, which limits their practical application in wastewater treatment.[6] To overcome this obstacle, researchers have previously tried to introduce a magnetic medium into biochar matrix which would enable one to use an external magnetic field to conduct an easy solid–liquid separation. If successful, this technique would represent a major step towards the true commercialization of biochar-based absorbents.[7]

Various types of magnetic particles have been employed to attain magnetic properties of biochar in recent years, such as $Fe_3O_4$,[8] $\gamma$-$Fe_2O_3$,[9] $CoFe_2O_4$.[10] Among these media, zerovalent iron (ZVI) has attracted some of the greatest interest due to its powerful magnetic and reducing properties. So far, biochar supported ZVI composites have been successfully synthesized and demonstrated to be excellent adsorbents for the remediation of wastewater contaminated with acid orange 7, trichloroethylene and pentachlorophenol.[11–13] However, to date, the preparation of these ZVI/biochar composites has mainly been carried out using a series of time-consuming and costly steps, including wet impregnation of preprocessed biochar, liquid-phase reduction of ferrous iron salt by borohydride. The complicated nature of these synthetic processes limited the large-scale application of ZVI/biochar composites. Therefore, developing simple synthesis procedures for ZVI/biochar composites is an area of high priority research.

Moreover, there is currently an interest in the use of magnetic carbon materials with high saturation magnetization ($M_s$), which are not only sufficient for conventional magnetic separation, but also desirable for use in high-end biomedical, ferrofluid and other applications.[14,15] However, to the authors' knowledge, there is no report on the synthesis of magnetic biochar with high $M_s$. As biochar is carbon-enriched, low-cost

[a]*International Centre for Bamboo and Rattan, Beijing, 100102, China. E-mail: liuxe@icbr.ac.cn; Tel: +86 1084789712*

[b]*School of Forestry and Landscape Architecture, Anhui Agricultural University, Hefei, 230036, China*

[c]*Forest Products Laboratory, Forest Service, Madison, WI 53726-2398, USA*

† Electronic supplementary information (ESI) available. See DOI: 10.1039/c5ra13236c

and easily available, using biochar as both a starting material and an iron-reduced agent to attain ZVI/biochar composites with high $M_s$ could be a very promising synthesis strategy that has yet to be explored.

In this research, three magnetic bamboo charcoal composites were prepared by mixing Moso bamboo charcoal powder with aqueous ferric chloride solution and subsequently pyrolyzing under different high temperatures (800, 1000 and 1200 °C), then characterized using X-ray powder diffraction (XRD), X-ray photoelectron spectroscopy (XPS), field emission scanning electron microscopy (FESEM), energy dispersive X-ray spectroscopy (EDAX), high-resolution transmission electron microscopy (HRTEM), Raman spectroscopy and superconducting quantum interference device (SQUID). The former is a $Fe_3O_4$/α-$Fe_2O_3$/bamboo charcoal composite and the latter two are both ZVI/bamboo charcoal composites with high $M_s$. Based on the observation of structures and morphologies of different products, a potential formation mechanism of ZVI/bamboo charcoal composites is presented.

## 2. Materials and methods

### 2.1 Materials

Three-year-old Moso bamboo powder (collected from Taipin Experimental Station, Anhui Province, China) was used as a biomass feedstock to prepare magnetic bamboo charcoal composites. The analytic grade ferric chloride hexahydrate ($FeCl_3 \cdot 6H_2O$) was purchased from Alfa Aesar Inc. (China). All chemical solutions were prepared using deionized (DI) water with a resistivity of 18.2 MΩ $cm^{-1}$, which was also used to rinse and clean the samples.

### 2.2 Preparation of magnetic bamboo charcoal composites

The magnetic bamboo charcoal composites were prepared by using a typical procedure as shown in Scheme 1. Bamboo powder was first pyrolyzed in a tube furnace at a temperature of 600 °C for one hour at the heating rate of 5 °C $min^{-1}$ under argon (Ar) gas flow of 300 mL $min^{-1}$. The resulting bamboo charcoal was stored in an air-tight container for further use.

The suspension of bamboo charcoal with $Fe^{3+}$ was prepared by dissolving four grams of the resulting charcoal powder and forty grams of $FeCl_3 \cdot 6H_2O$ in 60 mL DI water in a breaker first, then agitated at 350 rpm with a magnetic stirrer to maintain a uniform concentration and dried at 80 °C for 3 h in an oven. The obtained solid mixture was ground with a mortar to obtain a very fine powder.

Three pre-treated specimens of four grams each were finally magnetized. The sample was pyrolyzed at 800 °C (or 1000 and 1200 °C) for one hour at the heating rate of 5 °C $min^{-1}$ with the above-mentioned flow rate of Ar gas. After being cooled naturally to room temperature inside the furnace, the resulting samples were collected and stored in an air-tight container for further use. These obtained products are referred to as MBC800, MBC1000 and MBC1200, respectively, where the suffix number represents the pyrolytic temperature.

### 2.3 Characterization

Using Cu-Kα radiation over the $2\theta$ range of 5–80°, XRD analysis was carried out with a computer-controlled X-ray diffractometer (Philips Electronic Instruments) to identify crystallographic structures and mineral composition in the samples. To investigate the surface chemistry, XPS measurements were performed on an ESCALAB 250Xi spectrometer (Thermo Fisher Scientific) using a monochromatic AlKα X-ray (1486.6 eV) source. Raman spectra were recorded at ambient conditions using a confocal Raman microscope (HR-800, Horiba Jobin Yvon) equipped with an exciting laser source emitting at 633 nm (red laser). An integration time of 30 s was chosen for each measurement to achieve spectra with good counting rates. The laser power of the incident beam measured at the sample position was kept at 5 mW to prevent irreversible thermal damage to the specimen surface. The morphologies and elemental analysis of the investigated samples were examined by a FESEM (FEI XL-30, with an accelerating voltage at 20 kV) equipped with an EDAX (FEG 132-10). Prior to TEM analysis undertaken by a JEM-2100 at 200 kV, the samples were dripped onto a copper grid covered with a carbon film after ultrasonication for 20 min in dispersant (ethanol). The magnetic properties were investigated using a superconducting quantum interference device (SQUID) magnetometer from Quantum design. All the

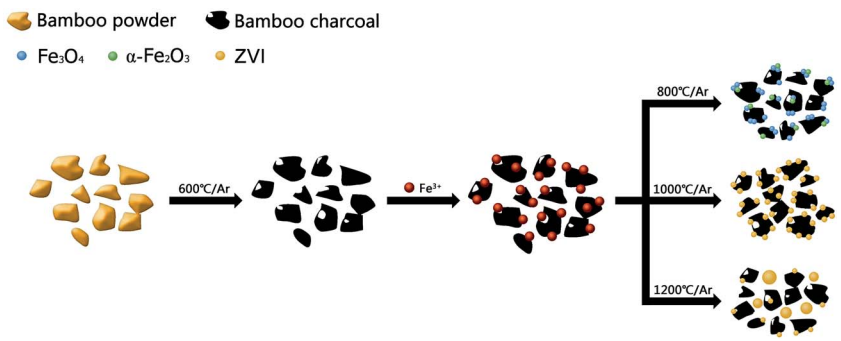


Scheme 1 Illustration of strategy for preparation of magnetic bamboo charcoal composites.

measurements were performed on powder forms of the samples after vacuum drying.

## 3. Results and discussion

### 3.1 Structure analysis

The XRD patterns for MBC800, MBC1000 and MBC1200 are shown in Fig. 1. Strong and sharp reflection XRD peaks suggested that metal or metallic compounds in the three as-prepared magnetic bamboo charcoal composites were all well crystallized.

Fig. 1a gives the XRD pattern of MBC800. Major diffraction peaks can be seen at $2\theta = 18.4°$, 30.2°, 35.5°, 37.1°, 43.2°, 53.5°, 57.3°, 62.9°. These distinct peaks correspond to eight indexed planes (111), (220), (311), (222), (400), (422), (511) and (440) of magnetite (JCPDS card no. 74-0748). However, several planes, *i.e.* (220), (311), (400), (422), (511) and (440), can also be indexed as maghemite with a spinel structure.[16,17] To further distinguish the valence state of iron in MBC800, the XPS spectra were measured. Several peaks shown in the survey spectrum (Fig. 2a) imply the presence of carbon (C 1s), oxygen (O 1s) and iron (Fe 2p) elements, which would have come from the carbon and iron oxide in MBC800, respectively.[18] As shown in Fig. 2b, the two peaks at 724.32 and 711.02 eV can be assigned to the binding energies of Fe $2p_{1/2}$ and Fe $2p_{3/2}$, respectively, which are close to the reported values of $Fe_3O_4$ in other available literature.[19] Simultaneously, there is no charge transfer satellite structure of Fe $2p_{3/2}$ at around 720 eV indicating the presence of a mixed oxide of Fe(II) and Fe(III).[20] Additionally, a nonlinear curve fit, with a Gaussian–Lorentzian mix function and Shirley background subtraction, was used to deconvolute the Fe 2p XPS spectrum. The investigation of multiplet splitting shows that Fe 2p envelope can be well fitted using peaks from both Fe(II) and Fe(III) constrained to be at 709.8 and 722.8 eV as well as 711.2 and 724.3 eV, respectively, based on the binding energies as reported by Graat and Somers.[21] Thus, these results provide more evidence for the argument that the detected crystalline iron oxide in MBC800 by XRD analysis is multivalent $Fe_3O_4$ rather than $\gamma$-$Fe_2O_3$.

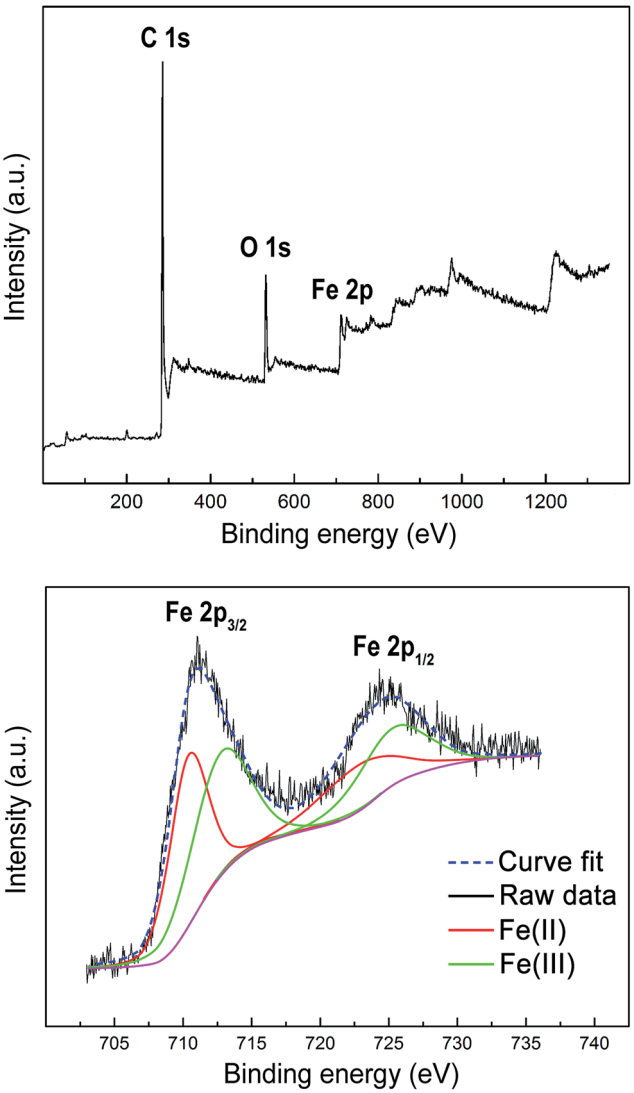


Fig. 2 XPS spectrum of the MBC800: (a) survey spectrum and (b) high-resolution Fe 2p binding energy spectrum.

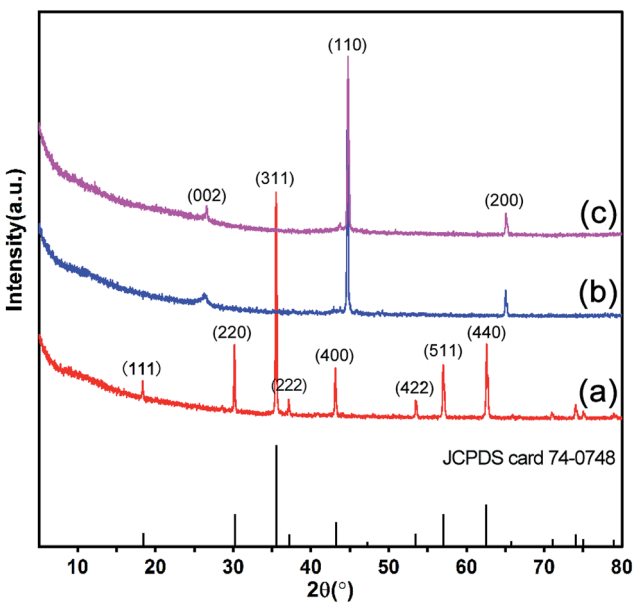


Fig. 1 XRD patterns of (a) MBC800, (b) MBC1000 and (c) MBC1200.

The XRD patterns of MBC1000 and MBC1200 are almost identical and ZVI is identified as the major crystalline phase. The peaks at 44.8° and 65.1° corresponding to the crystal planes of (110) and (200) respectively indicate the formation of ZVI,[22] while the peak centered at $2\theta = 26.5°$ can be attributed to the (002) reflex of partially graphitized carbon,[23] which in turn is due to the carbonization of bamboo char and the presence of iron giving carbon structures with some degree of graphitic order.[24] What is more, the full width at half maximum (FWHM) of the most intense (110) reflection can be used as an indicator of crystallinity (crystal size/disorder, which is inversely related to FWHM). XRD data shows that the crystallinity of ZVI is better in MBC1000 (FWHM = 0.150° in $2\theta$) than in MBC1200

(FWHM = 0.185° in 2$\theta$). Moreover, the ZVI crystallite dimension was determined from the XRD patterns using the Debye–Scherrer equation:

$$D = \frac{k\lambda}{\beta \cos \theta} \quad (1)$$

where $D$ is the mean size of the ZVI nanocrystals, $\lambda$ is the X-ray wavelength (0.15418 nm), $k$ is the Debye–Scherrer constant (0.89), $\beta$ is the FWHM and $\theta$ is the Bragg diffraction angle. The calculated results show that the mean size of ZVI crystallite in MBC1000 and MBC1200 are 28.5 and 23.2 nm, respectively.

The Raman spectra of all the specimens shown in Fig. 3 indicate the presence of the graphite and disordered amorphous carbon in the samples. The Raman spectrums obtained with all MBC samples mainly exhibit two strong peaks at the D- and G-bands. The D-band was the Raman band at a shift of around 1330 $cm^{-1}$ corresponding to a stretching vibration mode of amorphous carbon and the G-band at a shift of around 1591 $cm^{-1}$ was attributed to a stretching vibration mode of graphite C=C bonds.[25] The peak area ratio of G-band to D-band ($A_G/A_D$) for MBC800, MBC1000 and MBC1200 were calculated to be 7.8%, 36.7% and 38%, respectively. The $A_G/A_D$ ratios in the Raman spectra of MBC1000 and MBC1200 are significantly higher than that of MBC800, implying that a more uniform carbonaceous structure (graphite) formed after thermal treatment. These results also agree with the XRD data.

Finally, the Raman diffraction peaks of MBC800 from 200 to 800 $cm^{-1}$ provide additional information on the structure. The characteristic peak at 661 $cm^{-1}$ corresponding to one $A_{1g}$ vibration mode of $Fe_3O_4$ creates a consensus on the former XRD and XPS analyses. However, the four Raman scattering peaks at 228, 294, 407 and 497 $cm^{-1}$, can be accredited to the $A_{1g}$, $E_g$, $E_g$ and $A_{1g}$ modes respectively and these peaks clearly designate $\alpha$-$Fe_2O_3$.[26] It needs to be pointed that the absence of any $\alpha$-$Fe_2O_3$ diffraction peak from the XRD pattern of MBC800 (Fig. 1a) does not rule out the formation of $\alpha$-$Fe_2O_3$, due to detection limitations of the XRD technique and, or, the amorphous structure of $\alpha$-$Fe_2O_3$.[27]

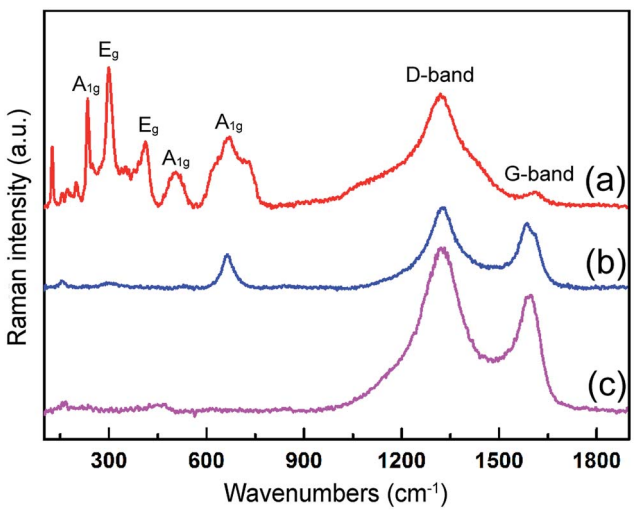


Fig. 3 Raman spectra of (a) MBC800, (b) MBC1000 and (c) MBC1200.

### 3.2 Morphological investigations

FESEM images of the respective synthesized samples at different magnifications are presented in Fig. 4a, c and e. Meanwhile, EDAX elemental mapping images (Fig. 4b, e and f) show the general distribution of C and Fe elements in each composite.

It can be seen from Fig. 4a that quantities of sphere-like aggregates (mean size of approximately 5.0 μm) attached onto the surface of bamboo charcoal in MBC800. The majority of these aggregates appear to be formed by some smaller particles, which should be hybrids of $Fe_3O_4$ and $\alpha$-$Fe_2O_3$. Fine ZVI particles with diameter changing from micro-scale to nano-scale are well defined and embedded in the char matrix of MBC1000, as shown in Fig. 4c, thereby indicating a better adhesion of magnetic particles than MBC800. With regard to MBC1200, Fig. 4e illustrates that bigger spheres with diameter changing from 20.0 to 50.0 μm have been grown, which are independent of bamboo charcoal matrix. On top of that, Fig. 4f shows that there are a few smaller non-spherical particles with irregular surface still stuck to the original char.

In truth, nano-sized crystalline particles are clearly observed from HRTEM images (Fig. S1†), though FESEM images indicate that the dimension of magnetic particles in all the samples is

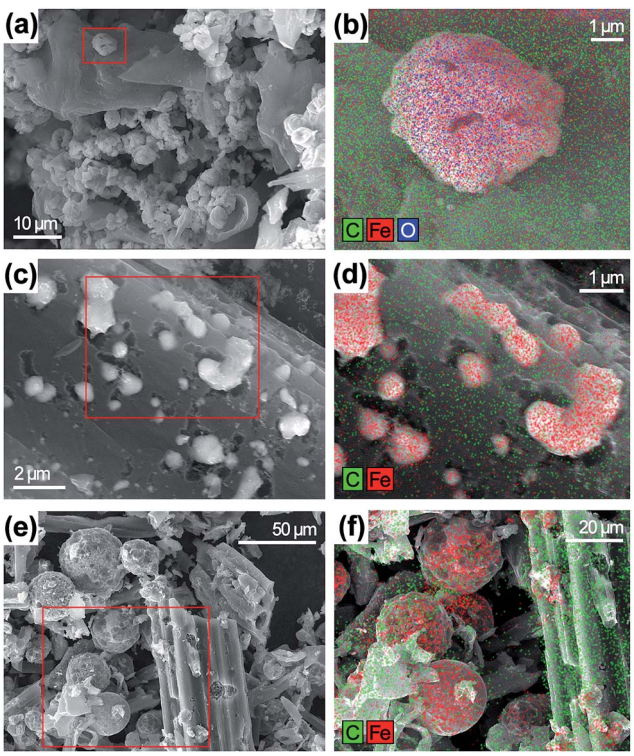


Fig. 4 FESEM and EDAX elemental mapping images of (a and b) MBC800, (c and d) MBC1000 and (e and f) MBC1200.

dominantly in the microscale. This should be due to the aggregation of abundant nano-sized particles with varying degrees in the final products.

### 3.3 Formation mechanism of ZVI/bamboo charcoal composites

In this study, ZVI/bamboo charcoal composites with high $M_s$ were obtained by carbonizing the Fe(III) salts/bamboo charcoal composites under 1000 or 1200 °C for one hour. No additional impurities were adopted during the synthetic process. A potential formation process was proposed with FESEM micrographs and phase change analyses.

Since the iron chloride was dissolved with the bamboo charcoal in water under ambient conditions, *i.e.*, atmospheric 20% $O_2$, it was probable that the formation of colloidal iron hydroxides and oxides occurred during the dissolution and agitation in water, which was modulated by the acidic nature of the iron chloride, possible pH effects of the charcoal and a continuous process of drying and crystallization. Therefore, the Fe species in the forms of hydroxides and oxides were uniformly dispersed on the surface of bamboo charcoal matrix at the end of oven drying.

Different chemical reactions between the precursors and char matrix took place in the course of anaerobic pyrolysis. EDAX analysis (Fig. S2†) suggests the presence of O and small amounts of remaining Cl in MBC800. However, only carbon and iron can be found in MBC1000 and MBC1200. Hence, it is possible to infer that, the Fe species at an early stage decomposed into solid $Fe_3O_4$, $\alpha$-$Fe_2O_3$ and gases such as HCl, $CO_2$, which were directly blown away by the flowing Ar gas. All the iron oxides turned into ZVI when the temperature is high enough (*e.g.* 1000 °C), due to the constantly increased activity of carbon atoms with good reducibility and contact area between bamboo charcoal and magnetic particles. It has been reported that $Fe_2O_3$ can be converted to other reduced species in the sequential reactions with solid carbon,[28–30] the equations (eqn (2) and (3)) of which may be applicable to this work.

$$6Fe_2O_{3(s)} + C_{(s)} \rightarrow 4Fe_3O_{4(s)} + CO_{2(g)} \quad (2)$$

$$Fe_3O_{4(s)} + 2C_{(s)} \rightarrow 3Fe^0_{(s)} + 2CO_{2(g)} \quad (3)$$

While the pyrolysis temperature reached 1000 °C, ZVI particles grew and partially embedded in bamboo charcoal due to the reduction of the iron oxides. With further temperature rise, these particles aggregated spontaneously into spherical ones with fewer number and larger volume, most of which ultimately broke away from char matrix. Part of the reason some irregular ZVI particles in MBC1200 were kept attached to the charcoal is the inadequate residence time or pyrolytic temperature.

### 3.4 Magnetic properties

$M_s$, remanent magnetization ($M_r$) and coercivity ($H_c$) are the most important parameters used for examining the magnetic properties of specimens. Fig. 5 shows the magnetic hysteresis loops of the three composites samples measured at room temperature using a SQUID in the field $H$ sweeping from −10 000 to 10 000 Oe. Corresponding $M_s$, $M_r$ and $H_c$ values of each sample are tabulated in Table 1, from which it is found that the $M_s$ values follow the order of MBC1200 > MBC1000 > MBC800, in accordance with their pyrolytic temperature. Moreover, both MBC1000 and MBC1200 present superparamagnetic behavior, considering the coercivity lower than the theoretical value for superparamagnetic particles ($H_c \leq 50$ Oe).[31] The marginally higher coercivity of MBC800 may stem from the presence of different magnetic media (*i.e.* magnetite and hematite) in MBC800 which increases the degree of anisotropy.[32]

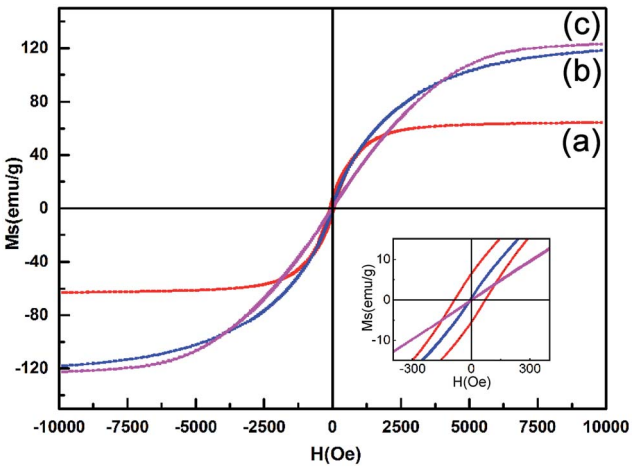


Fig. 5 Magnetic hysteresis curves of (a) MBC800, (b) MBC1000 and (c) MBC1200.

Table 1 The magnetic parameters of magnetic bamboo charcoal composites

| | Magnetic parameters | | |
|---|---|---|---|
| Samples | $M_s$ (emu g$^{-1}$) | $M_r$ (emu g$^{-1}$) | $H_c$ (Oe) |
| MBC800 | 63.6 | 6.3 | 83.4 |
| MBC1000 | 118.1 | 1.3 | 17.2 |
| MBC1200 | 122.7 | 0.3 | 8.9 |

The $M_s$ value of MBC800 is lower than that of bulk $Fe_3O_4$ (92 emu g$^{-1}$)[33] due to the smaller $Fe_3O_4$ particle size and the existence of non-magnetic carbon and weakly magnetic $\alpha$-$Fe_2O_3$. According to Tao *et al.*, the increase in the $M_s$ is attributable to an increase in crystallinity.[34] However, the $M_s$ value of MBC1200 is slightly higher than that of MBC1000, even though the crystallinity of ZVI in the latter is higher. The reason leading to such a result might be the aggregation effect of ZVI nanoparticles.[35] Besides, taking into account the relatively low $M_s$ values of magnetic cottonwood biochar (69.2 emu g$^{-1}$),[36] magnetic undigested sludge biochar (13.6 emu g$^{-1}$),[28] magnetic oak wood and oak bark biochar (8.87, 4.47 emu g$^{-1}$),[37] magnetic corn stover biochar (5.1 emu g$^{-1}$),[38] the magnetic properties of MBC1000 and MBC1200 are rather high. Furthermore, each

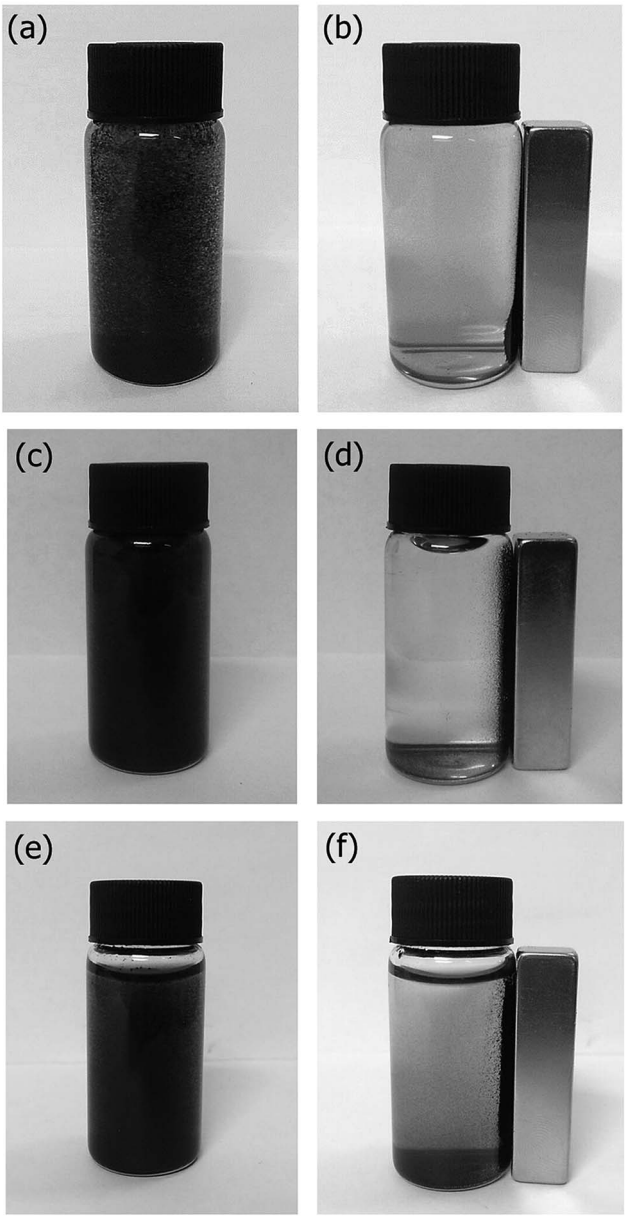


Fig. 6 Photographs of magnetic separation process of (a and b) MBC800, (c and d) MBC1000 and (e and f) MBC1200.

product uniformly dispersed in DI water exhibited prompt response to the external magnet (Fig. 6), highlighting the practicality of this technique for potential commercial applications in the future. It is notable that the aqueous solution of MBC1200 under the affinity of magnet was still slightly turbid, as shown in Fig. 6f. This is because a certain portion of bamboo charcoal in MBC1200 is separated from ZVI particles and not magnetized, which is also consistent with the FESEM results.

## 4. Conclusions

A rational synthesis of ZVI/bamboo charcoal composites with excellent magnetic properties has been demonstrated by mixing Moso bamboo charcoal powder with aqueous ferric chloride solutions and subsequently pyrolyzing under different high temperatures. The final products were characterized by XRD, XPS, FESEM, HRTEM, EDAX, Raman and SQUID analyses. A comparative study of their structural, morphological and magnetic properties has also been carried out. Findings from these analyses confirm that pyrolytic temperature plays an important role in controlling the component, shape and size of magnetic particles. Two magnetic media, *i.e.*, magnetite and hematite, are found to coexist in MBC800 and ZVI is the major magnetic phase of MBC1000 and MBC1200. The easy separation from aqueous solution by using an external magnet shows that all these iron-containing bamboo charcoal composites possess high water-dispersibility and good magnetic behaviour. They could have potential applications not only for sewage treatment, but also in biomedical and ferrofluid fields. Therefore, this novel study provides a platform for vastly increasing the applications of bamboo charcoal.

## Acknowledgements

This work was supported by the National Science-technology Support Plan Project (2012BAD54G0103). The support is gratefully acknowledged.

## Notes and references

1 B. Chen, Z. Chen and S. Lv, *Bioresour. Technol.*, 2011, **102**, 716.
2 Y. N. Chen, L. Y. Cha and Y. D. Shu, *J. Hazard. Mater.*, 2008, **160**, 168.
3 D. Mohan, C. U. Pittman Jr, M. Bricka, F. Smith, B. Yancey, J. Mohammad, P. H. Steele, M. F. Alexandre-Franco, V. Gómez-Serrano and H. Gong, *J. Colloid Interface Sci.*, 2007, **310**, 57.
4 M. Inyang, B. Gao, Y. Yao, Y. Xue, A. R. Zimmerman, P. Pullammanappallil and X. Cao, *Bioresour. Technol.*, 2012, **110**, 50.
5 J. Zhang, H. Fu, X. Lv, J. Tang and X. Xu, *Biomass Bioenergy*, 2011, **35**, 464.
6 D. H. K. Reddy and S. Lee, *Colloids Surf., A*, 2014, **454**, 96.
7 M. Zhang, B. Gao, S. Varnoosfaderani, A. Hebard, Y. Yao and M. Inyang, *Bioresour. Technol.*, 2013, **130**, 457.
8 S. A. Baig, J. Zhu, N. Muhammad, T. Sheng and X. Xu, *Biomass Bioenergy*, 2014, **71**, 299.
9 S. Wang, B. Gao, A. R. Zimmerman, Y. Li, L. Ma, W. G. Harris and K. W. Migliaccio, *Bioresour. Technol.*, 2015, **175**, 391.
10 W. Wang, X. Wang, X. Wang, L. Yang, Z. Wu, S. Xia and J. Zhao, *J. Environ. Sci.*, 2013, **25**, 1726.
11 G. Quan, W. Sun, J. Yan and Y. Lan, *Water, Air, Soil Pollut.*, 2014, **225**, 2195.
12 J. Yan, L. Han, W. Gao, S. Xue and M. Chen, *Bioresour. Technol.*, 2015, **175**, 269.
13 P. Devi and A. K. Saroha, *Bioresour. Technol.*, 2014, **169**, 525.
14 D. Zhang, S. Wei, C. Kaila, X. Su, J. Wu, A. B. Karki, D. P. Young and Z. Guo, *Nanoscale*, 2010, **2**, 917.
15 J. Yang and Q. Chen, *Chin. J. Chem. Phys.*, 2008, **21**, 76.

 

16 H. Li, L. Qin, Y. Feng, L. Hu and C. Zhou, *J. Magn. Magn. Mater.*, 2015, **384**, 213.
17 Q. Han, Z. Liu, Y. Xu, Z. Chen, T. Wang and H. Zhang, *J. Phys. Chem. C*, 2007, **111**, 5034.
18 P. Wu, N. Du, H. Zhang, L. Jin and D. Yang, *Mater. Chem. Phys.*, 2010, **124**, 908.
19 T. Yamashita and P. Hayes, *Appl. Surf. Sci.*, 2008, **254**, 2441.
20 M. Descostes, F. Mercier, N. Thromat, C. Beaucaire and M. Gautier-Soyer, *Appl. Surf. Sci.*, 2000, **165**, 288.
21 P. C. J. Graat and M. A. J. Somers, *Appl. Surf. Sci.*, 1996, **100**, 36.
22 L. B. Hoch, E. J. Mack, B. W. Hydutsky, J. M. Hershman, J. M. Skluzacek and T. E. Mallouk, *Environ. Sci. Technol.*, 2008, **42**, 2600.
23 S. Zhang, M. Zeng, J. Li, J. Li, J. Xu and X. Wang, *J. Mater. Chem. A*, 2014, **2**, 4391.
24 Z. Sun, L. Wang, P. Liu, S. Wang, B. Sun, D. Jiang and F. S. Xiao, *Adv. Mater.*, 2006, **16**, 1968.
25 A. B. Fuertes, M. Camps Arbestain, M. Sevilla, J. A. Maciá-Agulló, S. Fiol, R. López, R. J. Smernik, W. P. Aitkenhead, F. Arce and F. Macias, *Aust. J. Soil Res.*, 2010, **48**, 618.
26 D. L. A. de Faria, S. Venâncio Silva and M. T. de Oliveira, *J. Raman Spectrosc.*, 1997, **28**, 873.
27 J. S. Li, H. J. Li, Y. Zhu, Y. X. Hao, X. Y. Sun and L. J. Wang, *Appl. Surf. Sci.*, 2011, **258**, 657.
28 L. Gu, N. Zhu, D. Zhang, Z. Lou, H. Yuan and P. Zhou, *Bioresour. Technol.*, 2013, **136**, 719.
29 C. D. Frost, F. von Blanckenburg, R. Schoenberg, B. R. Frost and S. M. Swapp, *Contrib. Mineral. Petrol.*, 2007, **153**, 211.
30 R. A. Crane and T. Scott, *J. Nanopart. Res.*, 2014, **16**, 2813.
31 L. Morel, S. I. Nikitenko, K. Gionnet, A. Wattiaux, J. Lai-Kee-Him, C. Labrugere, B. Chevalier, G. Deleris, C. Petibois, A. Brisson and M. Simonoff, *ACS Nano*, 2008, **2**, 847.
32 D. L. Leslie-Pelecky and R. D. Rieke, *Chem. Mater.*, 1996, **8**, 1770.
33 D. H. Han, J. P. Wang and H. L. Luo, *J. Magn. Magn. Mater.*, 1994, **136**, 176.
34 K. Tao, H. J. Dou and K. Sun, *Colloids Surf., A*, 2008, **320**, 115.
35 T. Phenrat, N. Saleh, K. Sirk, R. D. Tilton and G. V. Lowry, *Environ. Sci. Technol.*, 2007, **41**, 284.
36 M. Zhang, B. Gao, S. Varnoosfaderani, A. Hebard, Y. Yao and M. Inyang, *Bioresour. Technol.*, 2013, **130**, 457.
37 D. Mohan, H. Kumar, A. Sarswat, M. Alexandre-Franco and C. U. Pittman, *Chem. Eng. J.*, 2014, **236**, 513.
38 D. Mohan, S. Kumar and A. Srivastava, *Ecol. Eng.*, 2014, **73**, 798.